Gas Storage Performance Investigation of $\{Ln_3(2,4\text{-PDCH})(2,4\text{-PDC})_4 \cdot 11H_2O\}_n$ (Ln=La,Ce,Nd,Sm,Eu) Based on Industrial Internet of Materials

Zhu, Taoyun*[+]

Department of Chemistry, College of Science, Heihe University, Heihe City Heilongjiang, 164300 P.R. CHINA

ABSTRACT: *The current study focuses on gas storage performance using the industrial internet of materials. A series of inorganic-organic coordination polymers made by lanthanide (III) and asymmetric ligands the pyridine-2,4-dicarboxylate were prepared in hydrothermal synthesis. The goals of this study were to investigate the gas adsorption/desorption behaviors and to measure the surface areas of the as-synthesized samples. These materials possess BET (Brunauer-Emmett-Teller) surface areas of approximately 480-610 m^2/g, which is verified by the surface area measurement based on the N_2 adsorption at 77 K. The adsorption isotherm of H_2 at 77 K exhibited a stable uptake of 1.35w % both at low pressure and high pressure, providing evidence for the robust framework of compounds with 0.7 nm pore size. Especially, the Cerium ion compound shows the highest H_2 uptake of 154 cm^3/g (1.35 wt %) among other samples, which is relatively low in comparison with that of Al-TCBPB and Zn_4O $(BDC)_3$, but higher than that of Zn_4O $(BTB)_2$.*

KEYWORDS: *Inorganic-organic coordination polymers; Asymmetric ligand; Pyridine-2,4-dicarboxylate; Hydrothermal synthesis.*

INTRODUCTION

Owing to the possibility of combining their optical and magnetic characteristics, porous higher surface and framework structures, Metal-Organic Frameworks (MOFs), based on lanthanide with coordination polymers, have been at the center of attention, and have been used to make new functionalities [1-4]. These materials possess a unique structure, and they can be implemented in different materials that have functionalities as ion exchange, molecular recognition, and gas storage along with physical qualities because of 4f electrons of lanthanide ions [5-20]. It is well known that lanthanide ions possess a high affinity with hard donor atoms and ligands having oxygen or hybrid oxygen-nitrogen atoms, especially multicarboxylate ligands that are utilized for establishing intended architectures [21-38].

Porous coordination compounds have received considerable interest since they can be employed to store or separate gas molecules [39], and the need for hydrogen-storage materials is the main reason for this considerable interest. Compared to purely organic materials, such materials are easy to synthesize owing to their lower energy of activation for the formation of a bond between

***** *To whom correspondence should be addressed.*
+ E-mail: tian.zhu2000@inbox.ru ; 2240172968@qq.com
1021-9986/2021/2/605-614 10/$/6.00

the ligand and metal. Thus far, numerous proposals have been put forward regarding different kinds of components which can be conducive to forming channeled materials [40-49]. With the highest gas storage capacity, MOFs are now considered as promising materials. Moreover, when guest molecules are not present, the lattice ought to be highly stable, i.e., the lattice must have true porosity and exihibit stability at repeated guest addition/removal cycles [50, 51]. Especially, one of the favourable properties of porous inorganic coordinated materials is the high selectivity to small-molecule adsorbents [52-58].

In order to construct MOFs with lanthanide ions, pyridine-2,4-dicarboxylic acid (dipic) ligands were investiagted extensively and considred as effectual sensitizers for europium(II)and terbium(III). Recently, a series of coordination solid of lanthanide have been synthesized and determined structurally within the framework provided by the asymmetric organic template pyridine-2,4-dicarboxylic acid [59-64].

Here, our main goal is to investigate the adsorption/desorbtion behavior of the compounds, which are formed with the formula $\{Ln_3(2,4\text{-PDCH})(2,4\text{-PDC})_4 \cdot 11H_2O\}_n$ (2,4-pdc=pyridine-2, 4-dicarboxylic acid,Ln=La, Ce, Nd, Sm, Eu). These compounds show stable gas storage performance, as well as larger surface areas confirmed by BET measurement. In this study, the reaction solvent was adjusted to obtain a large number of products for testing.

EXPERIMENTAL SECTION

Syntheses

Under atmospheric pressure at 150℃, $\{Ln_3(2,4\text{-PDCH})(2,4\text{-PDC})_4 \cdot 11H_2O\}_n$ was synthesized hydrothermally for 72 h in a 40 mL Teflon-lined steel autoclave. The initial solution was prepared by mixing lanthanum nitrate ($La(NO_3)_3 \cdot 6H_2O$, $Ce(NO_3)_3 \cdot 6H_2O$) lanthanum chloride ($NdCl_3 \cdot 6H_2O$,$SmCl_3 \cdot 6H_2O$,$EuCl_3 \cdot 6H_2O$), pyridine-2, 4-dicarboxylic acid with a molar ratio of 3:5 and DMF(N,N-dimethyl form amide) 10 ml(total volume,15 mL) under hydrothermal reaction. The autoclave was cooled down slowly to room temperature, and colorless powder was produced (the Ce-III compound showed yellow, and the Nd-III compound showed light greenish blue). In this study, powder compounds, produced by the solvent selected by DMF, had more efficiency compared to the crystal compounds added to the deionized water solvent.

Table 1: Crystal data of $Eu_3(2,4\text{-PDCH})(2,4\text{-PDC})_4 \cdot 11H_2O\}_n$.

Empirical Formula	$C_{35}N_5H_{38}Eu_3O_{31}$
Crystal System	tetragonal
Lattice Parameters	a =b=9.506(3) Å
	c = 51.936(4) Å
	V =4693(2) $Å^3$
Space Group	$P4_1$(#92)
Z value	4
R factor	0.0313
Rw factor	0.0795

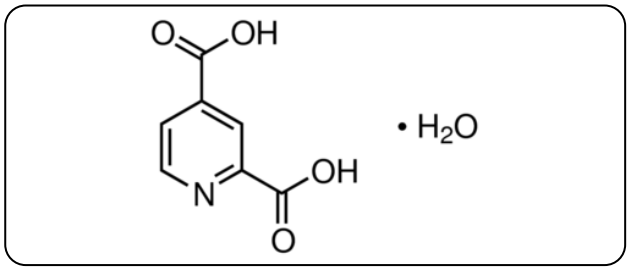

Molecular structure of the ligand pyridine-2,4-dicarboxylic acid, PDC

Characterization

By means of an Electron Probe Micro-Analysis (EPMA) employing a Shimadzu EPMA-8705, we carried out the quantitative and qualitative chemical analyses for the single crystal. By employing a Seiko Denshi TG-DTA 6300, Thermo Gravimetric Analysis (TGA) and Differential Thermal Analysis (DTA) were conducted at a heating rate of 5℃/min in the air. Shimadzu Corporation micrometrics Tristar-3000 was employed to perform the gas adsorption and specific surface area measurements.

RESULTS AND DISCUSSION

In this paper, the data related to the crystal compounds were synthesized and identified to illustrate their structure. Since five crystal compounds synthesized are isostructural, the details of the crystal structure are to be described here only for the Eu derivatives. Table 1 summarizes the crystallographic data and structure refinement parameters in detail.

By examining the compound structure thoroughly, it can be suggested that its crystal structure can be described

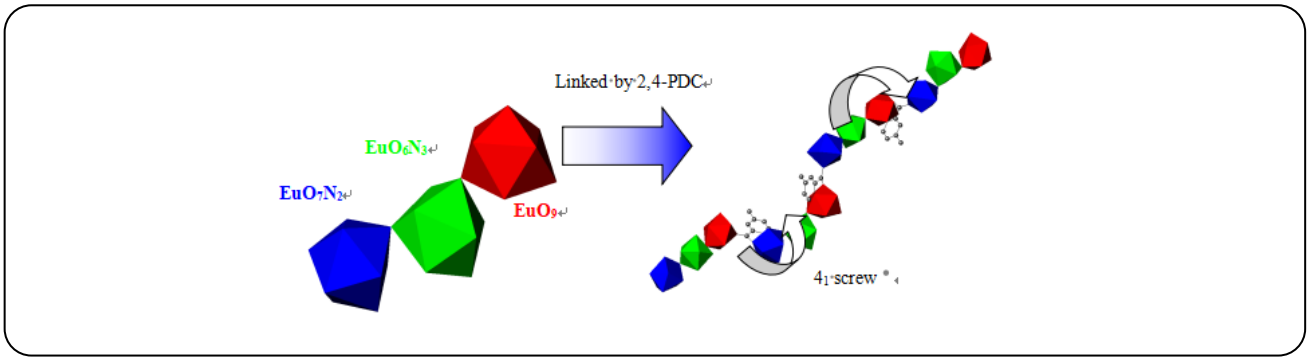

Fig. 1: Image of 1-D spiral chain consisted by three kinds of polyhedron of {Eu3(2,4-PDCH)(2,4-PDC)4 ·1H2O}n.

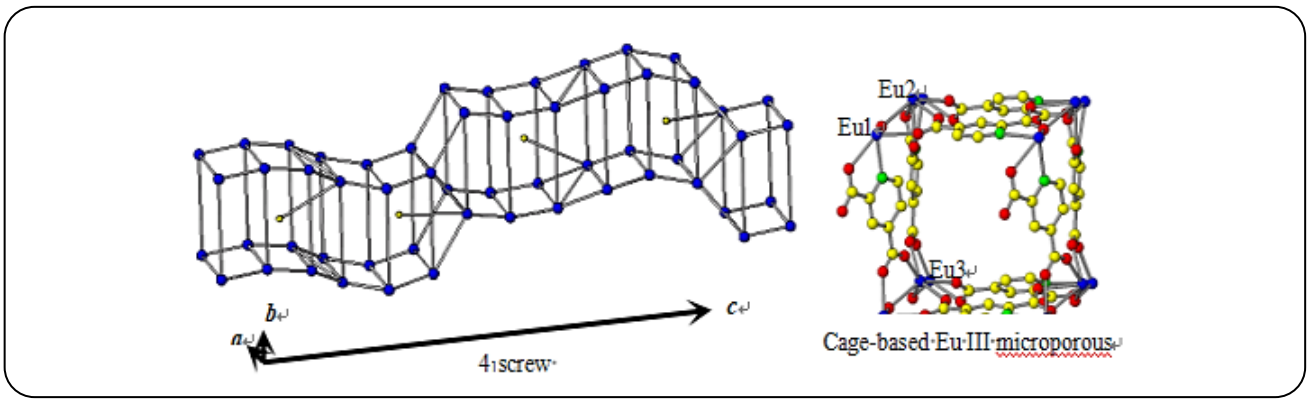

Fig. 2: Pattern diagram of distorted tetragonal tube of {Eu3(2,4-PDCH)(2,4-PDC)4 ·11H2O}n.

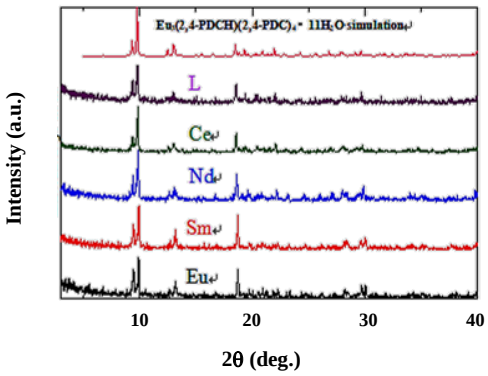

Fig. 3: Powder X-ray diffraction patterns for as-synthesized powder samples.

as distorted tetragonal tube constructed by spiral chains, which are made of [$Eu_3O_{22}N_5$] units from three types of nine-folded europium polyhedral with oxygen-sharing dipicolinic acid molecules. Each [$Eu_3O_{22}N_5$] cluster as well as each chain is bridged by carboxylate groups of the embedded dipic molecules to adjacent chains, thereby resulting in relatively large cavities within the tube to accommodate the crystal water (Figs. 1 and 2). To demonstrate the same structure by X-ray powder diffraction measurement, XRD measurements were carried out for the powder compounds synthesized in this paper (Fig. 3). The studies reveal that, similar to the simulation single-crystal sample, the pattern of the powder samples synthesized at 100℃ under reduced pressure, showing that the powder compounds have the same structure of the single-crystal owing to the good agreement of peaks.

The TG-DTA measurement was carried out from ambient temperature to 800 ℃ (Fig. 4). There exist two types of main weight loss in the temperature range mentioned above. The first one started at approximately 40℃ along with a negligible endothermic heat, which imply that the water molecules have been removed. All of the water molecules (eleven isolated water molecules) also had a weight loss and accommodated in the cage micro-pore in the compound. On the other hand, the weight loss at a high temperature, with 400℃ initiation temperature and 450℃ end temperature, is ascribed to the removal because of the combustion of four dipic molecules coordination with Eu III per unit formula. Otherwise,

Table 2: H_2 uptake and BET surface areas of MOF compounds reported at STP.

References	H_2 uptake [wt %]	BET surface area [m^2/g]	H_2 uptake / BET surface$\times10^{-3}$	Pore width [nm]	Ref.
Al-TCBPB	1.53	2311	0.66	1.18, 2.0	D. Saha et al., Hydrogen Energy (2012)
$Zn_4O(BTB)_2$	1.32	3275	0.40	1.27	D. Saha et al., Hydrogen Energy (2008)
$Zn_4O(BDC)_3$	1.46	2449	0.60	0.86	D. Saha et al., Sep. Tech.(2009)
Ce_3(2,4-PDCH) (2,4-PDC)$_4$	1.35	600	2.25	0.7	This study

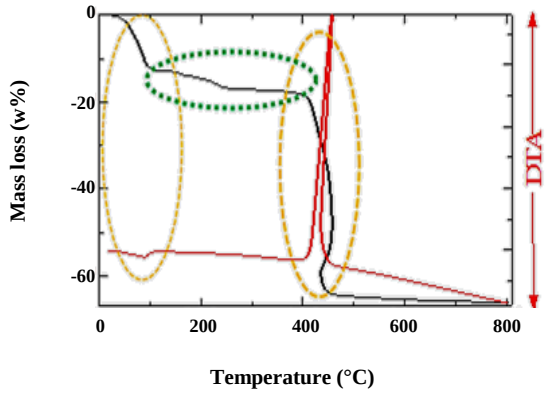

Fig. 4: TG-DTA curves for as-synthesized samples of {Eu_3(2,4-PDCH)(2,4-PDC)$_4$·11H_2O}$_n$.

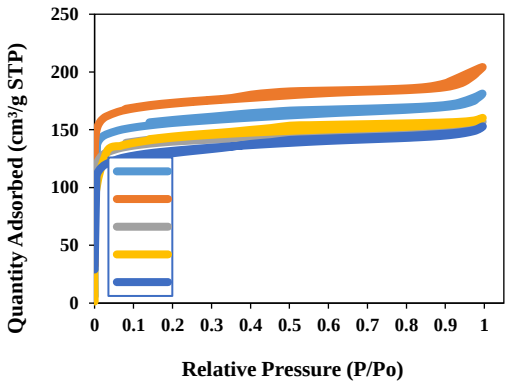

Fig. 5: adsorption and desorption isotherm of N_2 for Ln_3(2,4-PDCH)(2,4-PDC)$_4$·11H_2O.

it shows a slow slope down from 100℃ to 400℃, suggesting the weight loss of one dipic molecule linked to per [$Eu_3O_{22}N_5$] cluster.

Based on the results of TG-DTA, to confirm hydrogen storage ability of the as-synthesized samples, the nitrogen gas adsorption measurement was performed at 77 K on the as-synthesized sample and the dehydrated sample. The N_2 gas adsorption at 77 K clearly shows a reversible type I isotherm behavior after dehydration at 573 K, fitting the Langmuir equation, and a small amount of N_2 uptake was observed based on Scheme 5. It obviously proves that the samples have the micro-pore structure, however; hysteresis appeared to some extent over the saturation step. Furthermore, it revealed that the as-synthesized samples are narrow wedge-shaped porous structures because hysteresis curves belong to H4 (based on IUPAC) since the adsorption curves are almost parallel with the desorption curves. The adsorption isotherm of N_2 was used to compute the surface areas of samples, which are quite large compared to those of other samples reported (Table 2), which were estimated to be 480-610 m^2/g by applying the BET (Fig. 6), which is close to typical value microporous zeolites with high surface areas. Compared to other samples, the Ce compound is obviously superior in terms of both surface area and cell volume (according to as-synthesized crystal sample data).

In this study, pore size distribution analysis by HK methods using Ar gas at 87K(P/P0 = 0.0001~0.16) showed that there is a relatively narrow distribution of micropore at approximately 0.6-0.8 nm (Fig. 7) and considered to be an average value of 0.7 nm after a small change in the distance among lanthanide atoms for these samples. These pore sizes are consistent with the cages observed within the crystal structure data.

At 77 K, the adsorption isotherm of H_2 under low pressure displays a type I characteristic of a microporous material with no hysteresis and sharp adsorption (Fig. 8). The Ce sample shows the highest H_2 uptake of 154 cm^3/g (1.35 wt %) among other samples, which is relatively low compared to that of Al-TCBPB and Zn_4O $(BDC)_3$, but higher than that of $Zn_4O(BTB)_2$ (Table 2). On the other hand, compared to the adsorption isotherm of H_2 under low

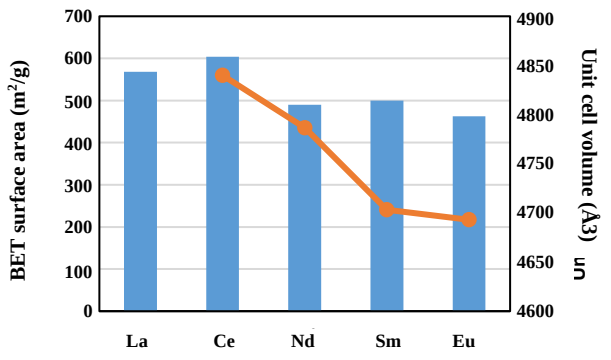

Fig. 6: BET surface areas and unit cell volumes of $Ln_3(2,4\text{-}PDCH)(2,4\text{-}PDC)_4 \cdot 11H_2O$.

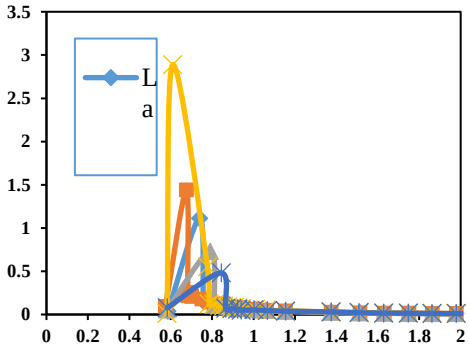

Ln	a [Å]
Ce	9.6225
Nd	9.5760
Sm	9.5167
Eu	9.5060

Fig. 7: Pore width distribution of $Ln_3(2,4\text{-}PDCH)(2,4\text{-}PDC)_4 \cdot 11H_2O$.

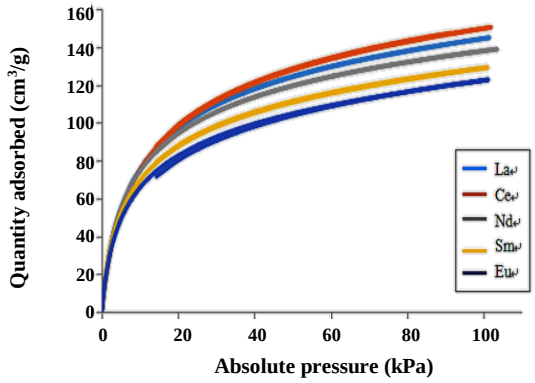

Fig. 8: Hydrogen adsorption of $\{Ln_3(2,4\text{-}Hdipic)(2,4\text{-}dipic)_4 \cdot 11H_2O\}_n$.

pressure, the H_2 adsorption of the Ce sample under high pressure was measured by self-designed apparatus in the laboratory (Fig. 9), and no significant change was observed in the H_2 uptake by increasing pressure. The saturation of the H_2 adsorption of 1.35w % at approximately 100 kPa can be the most feasible explanation for this.

In addition, in this study, since the Ce sample gas storage performance is superior compared to the MOFs reported, which is verified by test data and analysis (Table 3). Despite the fact that the surface areas of the as-synthesized sample are lower than those of the MOFs reported, the gas uptake clearly shows the porous metal-organic materials Ce III with complete retention of the host structures, providing evidence for a stable H_2 uptake (1.35 w%) both at low pressure and high pressure compared to others. This result may show the stable microporous structure framework (with pore size of about 0.7 nm), which is relatively suitable for the light gas storage [65-70].

CONCLUSIONS

In this paper, by investigating the surface areas and adsorption/desorption characteristics of the as-synthesized sample, it was demonstrated that implementing unsymmetrical organic templates in hydrothermal synthesis provides strong frameworks with promising properties to these coordination materials, which are ideal for gas storage. Based on these results, this study aims at investigating the selectivity of gas adsorption, such as CO_2, CH_4, C_2H_6, and SO_2, which might be compelling for investigating compounds allocated to viable applications, in which high surface areas are not required as opposed to stable gas storage performance.

Acknowledgments

The author would like to thank for the research support from the Sato and Toda Research Team, department of chemistry and chemical engineering faculty of engineering Niigata university. Especially, to be grateful to Prof. Mineo Sato, Prof. Kenji Toda and Mr. Kazuhiro Miura for their data and discussions.

This work was supported by a grant-in-aid for scientific research from the Heilongjiang Province Education Department Research program ((No.2018KYYWF1289)), a part of this work was also supported by the Doctor Initial Capital Program from Heihe University (No.2019KYQDJJYJ07).

Table 3: H_2 uptake and BET surface area of MOF compounds at low-hi-pressure and 77 K.

References	BET surface area [m^2/g]	H_2 uptake at 1 atm [wt%]	H_2 uptake at hi-pressure		Ref.
			Pressure [MPa]	Uptake [wt%]	
Al-TCBPB	2311	1.53	9	4.8	D. Saha et al., Hydrogen Energy (2012)
Zn_4O $(BTB)_2$	3275	1.32	12	11.0	D. Saha et al., Hydrogen Energy (2008)
Zn_4O $(BDC)_3$	2449	1.46	10	6.9	D. Saha et al., *Sep. Tech.*(2009)
Ce_3(2,4-PDCH) $(2,4\text{-PDC})_4$	600	1.35	4	1.35	

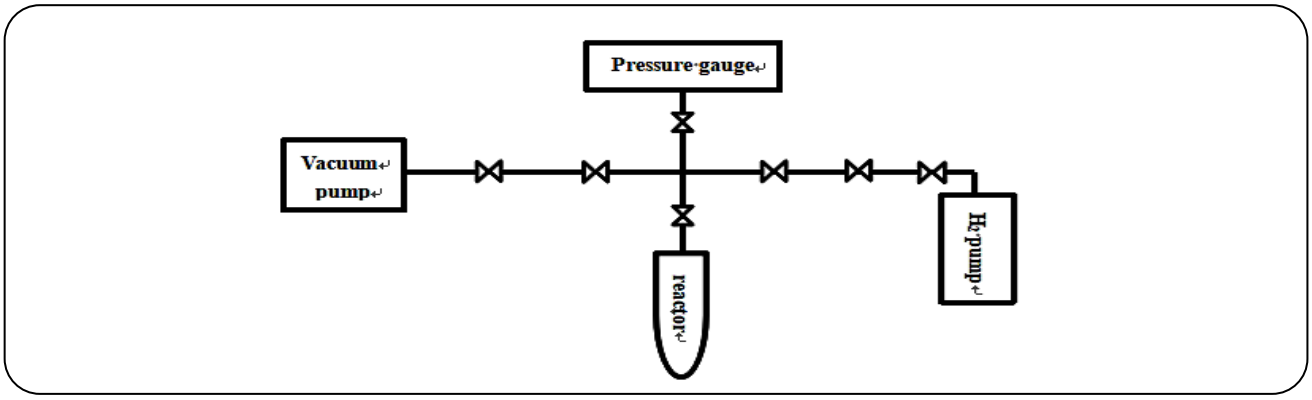

Fig. 9: Schematic diagram of apparatus used to measure hydrogen storage.

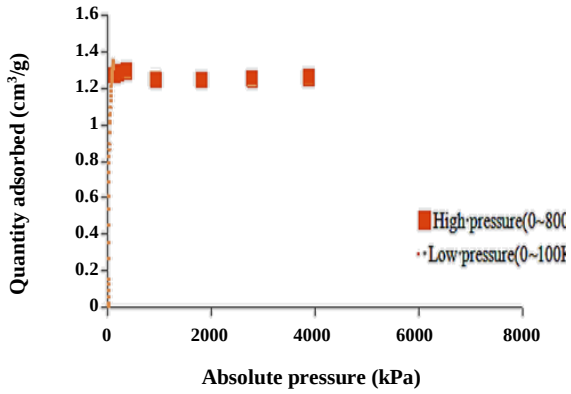

Fig. 10: H_2 adsorption of Ce_3(2,4-PDCH)(2,4-PDC)$_4$ ·11H_2O.

Received : Jan. 7, 2021 ; Accepted : Feb. 22, 2021

REFERENCES

[1] Heffern M.C., Matosziuk L.M., Meade T.J. Lanthanide Probes for Bioresponsive Imaging, *Chem. Rev.*, **114(8)**: 4496-4539 (2014).

[2] Ryu J., Lim S.Y., Park C.B., Photoluminescent Peptide Nanotubes, *Adv. Mater.*, **21(16)**: 1577-1581 (2009).

[3] Siqueira K.P.F., Lima P.P., Ferreira R.A.S., Carlos L.D., Bittar E.M., Matinaga F.M., Paniago R., Krambrock K., Moreira R.L., Dias A., Influence of the Matrix on the Red Emission in Europium Self-Activated Orthoceramics. *J. Phys. Chem. C.*, **119(31)**: 17825-17835 (2015).

[4] Lee D.E., Koo H., Sun I.C., Ryu J.H., Kim K., Kwon I.C., Multifunctional Nanoparticles for Multimodal Imaging and Theragnosis. *Chem. Soc. Rev.*, **41(7)**: 2656-2672 (2012).

[5] Binnemans K., Lanthanide-Based Luminescent Hybrid Materials. *Chem. Rev.*, **109**: 4283-4374 (2009).

[6] Hoffmans F., Cornelius M., Morell J., Froba M., Silica-Based Mesoporous Organic-Inorganic Hybrid Materials. *Angew. Chem. Int. Ed. Engl.*, **45**: 3216-3251 (2006).

[7] Pardo R., Zayat M., Levy D., Photochromic Organic-Inorganic Hybrid Materials. *Chem. Soc. Rev.*, **40**: 672-687 (2011).

[8] Zhao Y., Xie Z., Gu H., Zhu C., Gu Z., Bio-InspiredVariable Structural Color Materials. *Chem. Soc. Rev.*, **41**: 3297-3317 (2012).

[9] Feng J., Zhang H., Hybrid Materials Based on Lanthanide Organic Complexes: A Review. *Chem. Soc. Rev.*, **42**: 387-410 (2013).

[10] Bünzli J.C.G., On the Design of Highly Luminescent Lanthanide Complexes. *Coord. Chem. Rev.*, **293**: 19-47 (2015).

[11] Eliseevas V., Bunzli J.C., Lanthanide Luminescence for Functional Materials and Bio-Sciences. *Chem. Soc. Rev.*, 2010, 39: 189-227.

[12] Zhao H., Li Y., Song Q., Liu S., Ma Q., Ma L., Shu X., Catalytic reforming of volatiles from co-Pyrolysis of Lignite Blended with Corn Straw over Three Different Structures of Iron Ores, *J. Anal. Appl. Pyrolysis.*, **144**: 104714 (2019).

[13] Zhu W., Zhang Z., Chen D., Chai W., Chen D., Zhang J., Zhang C., Hao Y., Interfacial Voids Trigger Carbon-Based, All-Inorganic CsPbIBr 2 Perovskite Solar Cells with Photovoltage Exceeding 1.33 V. *Nano-Micro Lett.*, **12**: 1-4 (2020).

[14] Chen Y., He L., Li J., Zhang S., Multi-Criteria Design of Shale-Gas-Water Supply Chains and Production Systems Towards Optimal Life Cycle Economics and Greenhouse Gas Emissions under Uncertainty, *Comput. Chem.Eng.*, **109**: 216-235 (2018).

[15] Liu L., Li J., Yue F., Yan X., Wang F., Bloszies S., Wang Y., Effects of Arbuscular Mycorrhizal Inoculation and Biochar Amendment on Maize Growth, Cadmium Uptake and Soil Cadmium Speciation in Cd-Contaminated Soil. *Chemosphere*, **194**: 495-503 (2018).

[16] Zhang T., Wu X., Li H., Tsang D.C., Li G., Ren H., Struvite Pyrolysate Cycling Technology-Assisted by Thermal Hydrolysis Pretreatment to Recover Ammonium Nitrogen from Composting Leachate, *J. Clean. Prod.*, **242**: 118442 (2020).

[17] Li H., Zhang T., Tsang D.C., Li G., Effects of External Additives: Biochar, Bentonite, Phosphate, On Co-Composting for Swine Manure and Corn Straw, *Chemosphere*, **248**: 125927 (2020).

[18] Cai C., Wu X., Liu W., Zhu W., Chen H., Qiu J.C., Sun C.N., Liu J., Wei Q., Shi Y., Selective Laser Melting of near-α Titanium Alloy Ti-6Al-2Zr-1Mo-1V: Parameter Optimization, Heat Treatment and Mechanical Performance, *J. Mater. Sci. Technol.*, (2020).

[19] Cai C., Tey W.S., Chen J., Zhu W., Liu X., Liu T., Zhao L., Zhou K., Comparative Study on 3D Printing of Polyamide 12 by Selective Laser Sintering and Multi Jet Fusion, *J. Mater. Proc. Technol.*, **288**: 116882 (2021).

[20] Cai C., Gao X., Teng Q., Kiran R., Liu J., Wei Q., Shi Y., Hot Isostatic Pressing of a Near α-ti Alloy: Temperature optimization, Microstructural Evolution and Mechanical Performance Evaluation, *Mater. Sci. Eng.*, 140426 (2021).

[21] Simandl G.J., Geology and Market-Dependent Significance of Rare Earth Element Resources, *Mineralium Deposit.*, **49**(8): 889-904 (2014).

[22] Wang Y., Ye L., Wang T.G., Cui X.B., Shi S.Y., Wang G.W., Xu J.Q., Hydrothennal Syntheses and Characterizations of Two Novel Frameworks Constructed from Polyoxometalates, Metals and Organicunits, *Dalton Trans.*, **39(8)**: 1916-1919 (2010).

[23] Xiao L.N., Wang Y., Peng Y., Li G.H., Xu J.N., Wang L.M., Hu Y.Y., Wang T.G., Gao Z.M., Zheng D.F., Cui X.B., Xu J.Q., Hydrothermal Syntheses and Structures of Four New Polyoxometalate Based Supramolecular Architectures, *Inorganica Chimica. Acta.*, **387**: 204-211 (2012).

[24] Schwendemann T.C., May P.S., Berry M.T., Hou Y.Q., Meyers C.Y., Effect of Ligand Deuteration on the Decay of $Eu^{3+}(_5D_0)$ in Tris(2,2,6,6-tetramethyl-3,5-heptanedionato) Europium(III), *J. Phys. Chem. A.*, **102(45)**: 8690-8694 (1998).

[25] Humphrey S.M., Chang J.S., Jhung S.H., Yoon J.W., Wood P.T., Porous Cobalt(II)-Organic Frameworks with Corrugated Walls Structurally Robust Gas-Sorption Materials, Angew. *Chem. Int. Ed.*, **46**: 272-275 (2007).

[26] Kondo M., Okubo T., Asami A., Noro S.I., Yoshitomi T., Kitagawa S., Ishii T., Matsuzaka H., Seki K., Rational Synthesis of Stable Channel-Like Cavities with Methane Gas Adsorption Properties: $[\{(Cu_2(pzdc)_2(L)\}]_n$,(pzdc = pyrazine-2,3-dicarboxylate; L=a Pillar Ligand), *Angew. Chem. Int. Ed.*, **38(1-2)**: 140-143 (1999).

[27] Yoon J.W., Jhung S.H., Hwang Y.K., Humphrey S.M., Wood P.T., Chang J.S., Gas-Sorption Selectivity of CUK-1: A Porous Coordination Solid Made of Cobalt(II) and Pyridine-2, 4-Dicarboxylic Acid. *Adv. Mater.*, **19(14)**: 1830-1834 (2007).

[28] Daiguebonne C., Kerbellec N., Bernot K., Gérault Y., Deluzet A., Guillou O., Synthesis, Crystal Structure, and Porosity Estimation of Hydrated Erbium Terephthalate Coordination Polymers. *Inorg. Chem.*, **45**(14): 5399-5406 (2006).

[29] Koh K., Wong-Foy A.G., Matzger A.J., A Porous Coordination Copolymer with over 5000m^2/g BET Surface Area. *J. Am. Chem. Soc.*, **131**: 4184-4185 (2009).

[30] Kobayashi H., Ikarashi K., Uematsu K., Toda K., Okawa H., Taoyun Z., Sato M., One-Dimensional Channels Constructed from Hydrogen Bonding Networks Among 4, 4'-Bipyridine Units and Water Molecules Available for Accommodation of Poly - Oxomolybdate Clusters, *Inorg. Chim. Acta.*, **362**: 238-242 (2009).

[31] Zhao J., Shi D., Chen L., Ma P., Wang J., Zhang J., Niu J., Tetrahedral Polyoxometalate Nanoclusters with Tetrameric Rare-Earth Cores and Germanotungstate Vertexes, *Cryst. Growth Des.*, **13(10)**: 4368-4377 (2013).

[32] Han X.B., Zhang Z.M., Zhang T., Li Y.G., Lin W., You W., Su Z.M., Wang E.B., Polyoxometalate-Based Cobalt-Phosphate Molecular Catalysts for Visible Light-Driven Water Oxidation, *J. Am. Chem. Soc.*, **136(14)**: 5359-5366 (2014).

[33] Meinert L.D., Robinson G.R., Nassar N.T, Mineral Resources: Reserves, Peak Production and the Future, *Resources*, **5(1)**:14- (2016).

[34] Yan C., Zhao H., Perepichka D.F., Rosei, F., Lanthanide Ion Doped Upconverting Nanoparticles:Synthesis, Structure and Properties, *Small*, **12**: 3888- 3907 (2016).

[35] Hasegawa Y., Kitagawa Y., Nakanishi T., Effective Photosensitized, Elec- trosensitized, and Mechanosensitized Luminescence of Lanthanide Complexes. *NPG Asia Mater.*, **10**: 52-70 (2018).

[36] Prdius D., Mudring A.V., Rare Earth Metal-Containing Ionic Liquids, *Coord. Chem. Rev.*, **363**: 1-16 (2018).

[37] Chen P., Li Q., Grindy S., Holten-Andersen N., White-Light-Emitting Lanthanide Metallogels with Tunable Luminescence and Reversible Stimuli-Responsive Properties. *J. Am. Chem. Soc.*, **137**: 11590-11593 (2015).

[38] Li Y., Liu X., Yang X., Lei H., Zhang Y., Li B., Enhancing Up-Conversion Fluorescence with a Natural Bio-Microlens. *ACS Nano*, **11**: 10672-10680 (2017).

[39] Cesca T., Perotto G., Pellegrini G., Michieli N., Kalinic B., Mattei G., Rare-Earth Fluorescence Thermometry of Laser-Induced Plasmon Heating in Silver Nanoparticles Arrays, *Sci. Rep.*, **8(1)**: 1-9 (2018).

[40] Hasegawa Y., Kitagawa Y., Thermo-Sensitive Luminescence of Lanthanide Complexes, Clusters, Coordination Polymers and Metal-Organic Frameworks with Organic Photo- Sensitizers, *J. Mater. Chem. C.*, **7(25)**: 7494-7511 (2019).

[41] Zhang T., He X., Deng Y., Tsang D.C., Yuan H., Shen J., Zhang S., Swine manure Valorization for Phosphorus and Nitrogen Recovery by Catalytic–Thermal Hydrolysis and Struvite Crystallization, *Sci. Total Environ.*, **729**: 138999 (2020).

[42] Zhang T., He X., Deng Y., Tsang D.C., Jiang R., Becker G.C., Kruse A., Phosphorus Recovered from Digestate by Hydrothermal Processes with Struvite Crystallization And Its Potential as a Fertilizer, *Sci. Total Environ.*, **698**: 134240 (2020).

[43] Deng Y., Zhang T., Sharma B.K., Nie H., Optimization and Mechanism Studies on Cell Disruption and Phosphorus Recovery from Microalgae with Magnesium Modified Hydrochar in Assisted Hydrothermal System, *Sci. Total Environ.*, **646**: 1140-1154 (2019).

[44] Zhang T., Wu X., Fan X., Tsang D.C., Li G., Shen Y., Corn Waste Valorization to Generate Activated Hydrochar to Recover Ammonium Nitrogen from Compost Leachate by Hydrothermal Assisted Pretreatment, *J. Environ. Manage.*, **236**: 108-117 (2019).

[45] Han X., Zhang D., Yan J., Zhao S., Liu J., Process Development of Flue Gas Desulphurization Wastewater Treatment in Coal-Fired Power Plants Towards Zero Liquid Discharge: Energetic, Economic And Environmental Analyses, *J. Clean. Prod.*, 121144 (2020).

[46] Yang W., Pudasainee D., Gupta R., Li W., Wang B., Sun L., An Overview of Inorganic Particulate Matter Emission from Coal/Biomass/MSW Combustion: Sampling and Measurement, Formation, Distribution, Inorganic Composition and Influencing Factors, *Fuel Proc. Technol.*, 106657 (2020).

[47] Liu Y., Hu B., Wu S., Wang M., Zhang Z., Cui B., He L., Du M., Hierarchical Nanocomposite Electrocatalyst of Bimetallic Zeolitic Imidazolate Framework and MoS_2 Sheets for Non-Pt Methanol Oxidation and Water Splitting, *Appl. Catal. Environ.*, **258**: 117970 (2019).

[48] Wang M., Hu M., Li Z., He L., Song Y., Jia Q., Zhang Z., Du M., Construction of Tb-MOF-on-Fe-MOF Conjugate as a Novel Platform for Ultrasensitive Detection of Carbohydrate Antigen 125 and Living Cancer Cells, *Biosens. Bioelectr.*, **142**: 111536- (2019).

[49] Wang M., Hu M., Hu B., Guo C., Song Y., Jia Q., He L., Zhang Z., Fang S., Bimetallic Cerium and Ferric Oxides Nanoparticles Embedded Within Mesoporous Carbon Matrix: Electrochemical Immunosensor for Sensitive Detection of Carbohydrate Antigen 19-9. *Biosens. Bioelectr.*, **135**: 22-29. (2019).

[50] Huang C.H, Luo L., Chen TM., An Investigation on the luminescence and Ce^{3+}—Eu^{2+} Energy Transfer in $Ca_9Y(PO_4)_7$:Ce^{3+},Eu^{2+} Phosphor, *J. Electrochem. Soc.*, **158(11)**: J341-J344 (2011).

[51] Jodeyri Entezari A., Azin R., Nasiri A., Bahrami H., Investigation of Underground Gas Storage in a Partially Depleted Naturally Fractured Gas Reservoir, *Iran. J. Chem. Chem. Eng. (IJCCE)*, **29(1)**: 103-110 (2010).

[52] Sun J., Zhang X., Xia Z., Du H., Luminescent Properties of $LiBaPO_4$:RE (RE= Eu^{2+}, Tb^{3+}, Sm^{3+}) Phosphors for White Light-Emitting Diodes, *J. Appl. Phys.*, **111(1)**: 013101 (2012).

[53] Liu L., Li D., Ma Y., Shen H., Zhao S., Wang Y., Combined Application of Arbuscular Mycorrhizal Fungi and Exogenous Melatonin Alleviates Drought Stress and Improves Plant Growth in Tobacco Seedlings. *J. Plant Growth Regul.*, 1-14 (2020).

[54] Wang M., Yang L., Hu B., Liu J., He L., Jia Q., Song Y., Zhang Z., Bimetallic NiFe Oxide Structures Derived from Hollow NiFe Prussian Blue Nanobox for Label-Free Electrochemical Biosensing Adenosine Triphosphate. *Biosens. Bioelectr.*, **113**: 16-24 (2018).

[55] Kordestani H., Zhang C., Shadabfar, M., Beam Damage Detection Under a Moving Load Using Random Decrement Technique and Savitzky–Golay Filter, *Sensors*, **20(1)**: 243 (2020).

[56] Kordestani H., Zhang C., Direct use of the Savitzky–Golay Filter to Develop an Output-Only Trend Line-Based Damage Detection Method, *Sensors*, **20(7)**: 1983- (2020).

[57] Koizumi A., Hasegawa T., Itadani A., Toda K., Zhu T., Sato M., A New Lanthanum(III) Complex Containing Acetylacetone and 1H- Imidazole, *Acta Cryst.*, **E73**: 1739-1742 (2017).

[58] Koizumi A., Hasegawa T., Itadani A., Toda K., Zhu T., Sato M., Structure of triaquatris (1,1,1- triflouoro-4-oxopentan-2-olato) Cerium (III) as a Possible Fluorescent Compound, *Acta Cryst.*, **E74**, 229–232 (2018).

[59] Mousavi A.A., Zhang C., Masri S.F., Gholipour G., Structural Damage Localization and Quantification Based on a CEEMDAN Hilbert Transform Neural Network Approach: A Model Steel Truss Bridge Case Study. *Sensors*, **20(5)**: 1271 (2020).

[60] Zhang J., Liu B., A Review on the Recent Developments of Sequence-Based Protein Feature Extraction Methods, *Curr. Bioinform.*, **14(3)**: 190-199 (2019).

[61] Xu L., Jiang S., Zou Q., An in Silico Approach to Identification, Categorization and Prediction of Nucleic Acid Binding Proteins, *BioRxiv* (2020).

[62] Zhu J., Wu P., Chen M., Kim M.J., Wang X., Fang T., Automatically Processing IFC Clipping Representation for BIM and GIS Integration at The Process Level. *Appl. Sci.*, **10(6)**: 2009- (2020).

[63] Guo H., Qian K., Cai A., Tang J., Liu J., Ordered Gold Nanoparticle Arrays on the Tip of Silver Wrinkled Structures for Single Molecule Detection, *Sens. Actuat. Chem.*, **300**: 126846 (2019).

[64] Guo H., Li X., Zhu Q., Zhang Z., Liu Y., Li Z., Wen H., Li Y., Tang J., Liu J., Imaging Nano-Defects of Metal Waveguides Using the Microwave Cavity Interference Enhancement Method, *Nanotechnol.*, **31(45)**: 455203 (2020).

[65] Yan H., Xue X., Chen W., Wu X., Dong J., Liu Y., Wang Z., Reversible Na+ Insertion/Extraction in Conductive Polypyrrole-Decorated NaTi2 (PO4) 3 Nanocomposite with Outstanding Electrochemical Property. *Appl. Surf. Sci.*, **530**: 147295 (2020).

[66] Xu Q., Zou Z., Chen Y., Wang K., Du Z., Feng J., Ding C., Bai Z., Zang Y., Xiong Y., Performance of a Novel-Type of Heat Flue in a Coke oven Based on High-Temperature and Low-Oxygen Diffusion Combustion Technology, *Fuel.*, **267**: 117160 (2020).

[67] Zhong P.F., Lin H.M., Wang L.W., Mo Z.Y., Meng X.J., Tang H.T., Pan Y.M., Electrochemically Enabled Synthesis of Sulfide Imidazopyridines *Via* a Radical Cyclization Cascade. *Green Chem.*, **22(19)**: 6334-6339 (2020).

[68] Ali A., Iqbal M., K Khattak K., Pilot Plant Investigation on the Start-up of a UASB Reactor Using Sugar Mill Effluent, *Cent. Asian J. Environ. Sci. Technol. Innov.*, **1(4)**: 199-205 (2020).

[69] Liu H., Liu X., Zhao F., Liu Y., Liu L., Wang L., Geng C., Huang P., Preparation of a Hydrophilic and Antibacterial Dual Function Ultrafiltration Membrane with Quaternized Graphene Oxide as a Modifier, *J. Colloid Interface Sci.*, **562**: 182-192 (2020).

[70] Li X., Zhang R., Zhang X., Zhu P., Yao T., Silver-Catalyzed Decarboxylative Allylation of Difluoroarylacetic Acids with Allyl Sulfones in Water. *Chem. Asian J.*, **15**(7), 1175-1179 (2020).